# BEAM ENERGY AND COLLISION SPECIES DEPENDENCES OF PHOTON-INDUCED LEPTON PAIR PRODUCTION AT STAR*

Xiaofeng Wang

for the STAR Collaboration

Key Laboratory of Particle Physics and Particle Irradiation (MoE)
Institute of Frontier and Interdisciplinary Science
Shandong University, Qingdao, China
xwang1@rcf.rhic.bnl.gov

*Received 29 July 2022, accepted 9 October 2022, published online 14 December 2022*

We report on the measurements of low-$p_{\mathrm{T}}$ $e^+e^-$ and $\mu^+\mu^-$ pairs produced in noncentral Au+Au collisions at $\sqrt{s_{NN}} = 54.4$ GeV and $\sqrt{s_{NN}} = 200$ GeV at STAR. The measured yields can be well described by the lowest-order EPA-QED calculations for both types of lepton pairs. The $\sqrt{\langle p_{\mathrm{T}}^2 \rangle}$ of $e^+e^-$ pairs exhibits collision energy dependence, with a hint of possible final-state effects. The low-$p_{\mathrm{T}}$ $J/\psi$ spectra in isobaric collisions ($^{96}_{44}$Ru+$^{96}_{44}$Ru, $^{96}_{40}$Zr+$^{96}_{40}$Zr) at $\sqrt{s_{NN}} = 200$ GeV are also measured. Photoproduced $J/\psi$ are found to be sensitive to the charge of the colliding nuclei, but not to the details of the nuclear form factor or the impact parameter.

DOI:10.5506/APhysPolBSupp.16.1-A96

## 1. Introduction

Strongly interacting matter, known as the Quark–Gluon Plasma (QGP), can be created in relativistic heavy-ion collisions [1]. A major goal of the Relativistic Heavy-Ion Collider (RHIC) is to study the properties of the QGP [2]. Since dileptons are produced through the entire evolution of the hot, dense medium without interacting with it strongly, they are considered an ideal probe to study the QGP. The dileptons can also be produced via the $\gamma\gamma \to l^+l^-$ process [3] while $J/\psi$ can be produced in photon–nucleus interactions via Pomeron exchange [4]. In these latter cases, the initial photons are quantized from the extremely strong electromagnetic fields generated by the highly charged ions at ultra-relativistic speed. These processes: $\gamma\gamma \to l^+l^-$

* Presented at the 29$^{\mathrm{th}}$ International Conference on Ultrarelativistic Nucleus–Nucleus Collisions: Quark Matter 2022, Kraków, Poland, 4–10 April, 2022.

and $\gamma + A \rightarrow J/\psi + X$, in heavy-ion collisions, are typically studied in so-called ultra-peripheral collisions (UPCs) [5, 6] for which the impact parameter between the colliding nuclei is larger than twice the nuclear radius and there is no hadronic interaction between the nuclei. Recently, significant excesses of dilepton and $J/\psi$ yields at very low transverse momentum ($p_{\mathrm{T}}$) have been observed at RHIC [7–9] in peripheral hadronic heavy-ion collisions. These excesses may originate from coherent photon-induced interactions. Measurements of dilepton and $J/\psi$ production at very low $p_{\mathrm{T}}$ for different collision energies, collision species, and centralities can shed new light on the origin of the excess [10, 11].

In this contribution, we present invariant mass distributions of low-$p_{\mathrm{T}}$ $e^+e^-$ and $\mu^+\mu^-$ pairs production. The energy dependence of $\sqrt{\langle p_{\mathrm{T}}^2 \rangle}$ for $e^+e^-$ pairs and low-$p_{\mathrm{T}}$ $J/\psi$ excess yields are also shown. Theoretical predictions are compared with data.

## 2. Experiment and analysis

The data reported are collected with the STAR detector. The 200 and 54.4 GeV Au+Au collision data taken in 2011 and 2017, respectively, are used for the dielectron analysis. The dataset that the dimuon analysis uses is the 200 GeV Au+Au collision data taken in 2014. $J/\psi$ analysis uses Zr+Zr and Ru+Ru collisions at 200 GeV recorded in 2018. The main sub-detectors used are the Time Projection Chamber (TPC) [12] and the Time of Flight (TOF) [13]. The TPC is the main detector for charged-particle tracking, and it can also measure the ionization energy loss to provide charged-particle identification. The TOF is used to identify particles by measuring the flight time. By combining the TPC and TOF, electrons and muons can be identified with high purity. The like-sign distribution is used to estimate the combinatorial and correlated background, with the mixed-event technique used to correct the acceptance difference. After subtracting background from the unlike-sign distribution, the raw signal can be obtained, which is then corrected for detector effects. Finally, a Monte-Carlo simulation is applied to evaluate the hadronic cocktail contribution.

## 3. Results and discussion

### *3.1. Low-$p_{\mathrm{T}}$ $e^+e^-$ pair production in Au+Au collisions*

After statistically subtracting the hadronic cocktail contribution from the inclusive $e^+e^-$ pairs, the invariant mass distributions of excess pairs for $p_{\mathrm{T}} < 0.15$ GeV/$c$ are shown in Fig. 1 for $\sqrt{s_{NN}} = 54.4$ GeV and $\sqrt{s_{NN}} = 200$ GeV in different centralities. The invariant mass spectra are smooth and featureless even in the range of known vector mesons. This is a consequence of the quantum numbers of the two photons involved in the

Breit–Wheeler process where the helicity state $J_z = 0$ is absent for real photons but necessary for exclusive vector-meson production. These excesses are also consistent with the lowest-order EPA-QED predictions [15, 16] for the collision of linearly polarized photons quantized from the extremely strong electromagnetic fields generated by the highly charged Au nuclei at ultra-relativistic speed.

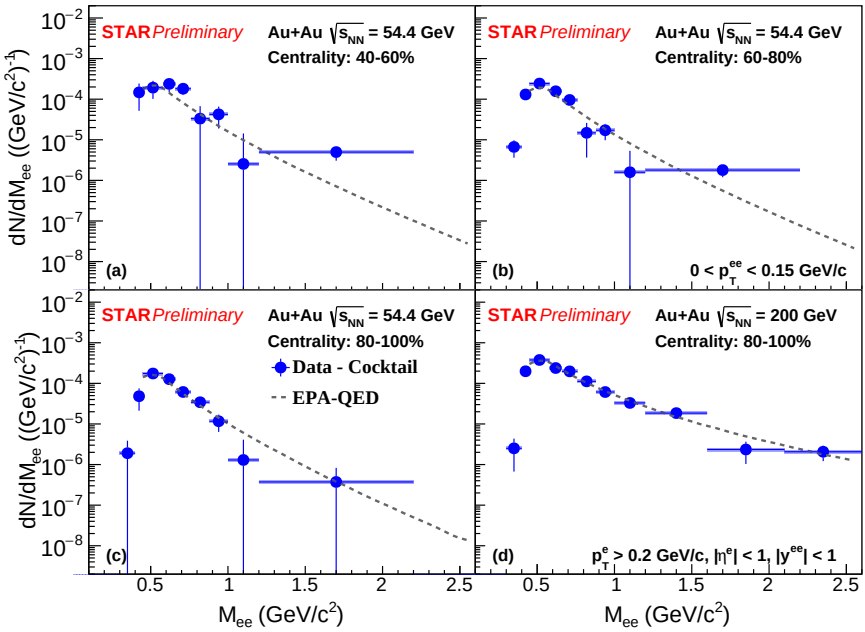


Fig. 1. (Color online) The low-$p_{\mathrm{T}}$ ($p_{\mathrm{T}} < 0.15$ GeV/$c$) $e^+e^-$ excess mass spectra (Data — Cocktail) within the STAR acceptance in Au+Au collisions at $\sqrt{s_{NN}} = 54.4$ GeV in the centrality of (a) 40–60%, (b) 60–80%, (c) 80–100%, and (d) $\sqrt{s_{NN}} = 200$ GeV in the centrality of 80–100% compared to the lowest-order EPA-QED predictions for $\gamma\gamma \to e^+e^-$ process (dashed line). Statistical uncertainties are shown as vertical bars on all points, while systematic uncertainties are shown as blue boxes which are smaller than the marker size.

Since $\sqrt{\langle p_{\mathrm{T}}^2 \rangle}$ is sensitive to $p_{\mathrm{T}}$ broadening, we study $\sqrt{\langle p_{\mathrm{T}}^2 \rangle}$ for $e^+e^-$ pairs as a function of beam energy in different centralities shown in Fig. 2. $\sqrt{\langle p_{\mathrm{T}}^2 \rangle}$ decreases with increasing impact parameter at both 54.4 and 200 GeV. For high precision results at $\sqrt{s_{NN}} = 200$ GeV in UPCs, the consistency between the EPA-QED prediction [15, 16] and our measurement shows that the EPA-QED predictions at $\sqrt{s_{NN}} = 200$ GeV can be treated as a baseline. $3.7\sigma$ difference is found when comparing all the data points at $\sqrt{s_{NN}} = 54.4$ GeV

to EPA-QED predictions at $\sqrt{s_{NN}} = 200$ GeV, which arises from the energy dependence of $\sqrt{\langle p_{\mathrm{T}}^2 \rangle}$ and possible final-state effects. $e^+e^-$ pairs produced from photon–photon interactions are mostly back to back, and final-state effects due to trapped magnetic field or Coulomb scattering in the QGP can lead to the observed $p_{\mathrm{T}}$ broadening.

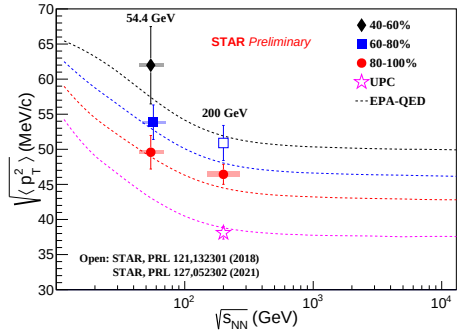


Fig. 2. The energy dependence of $\sqrt{\langle p_{\mathrm{T}}^2 \rangle}$ for $e^+e^-$ pairs compared to the lowest-order EPA-QED predictions shown as the dashed line in Au+Au collisions for the centrality intervals of 40–60%, 60–80%, 80–100%, and UPCs. Statistical uncertainties are shown as vertical bars, while systematic uncertainties are shown as boxes. Open markers are extracted from Refs. [7, 14].

### *3.2. Low-$p_{\mathrm{T}}$ $\mu^+\mu^-$ pair production in Au+Au collisions*

After statistically subtracting the hadronic cocktail contribution from the inclusive $\mu^+\mu^-$ pairs, the invariant mass distributions of excess pairs for $p_{\mathrm{T}} < 0.1$ GeV/$c$ are shown in Fig. 3 for $\sqrt{s_{NN}} = 200$ GeV in different

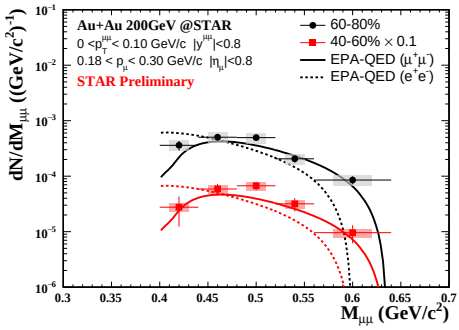


Fig. 3. The low-$p_{\mathrm{T}}$ ($p_{\mathrm{T}} < 0.1$ GeV/$c$) $\mu^+\mu^-$ excess mass spectra (Data — Cocktail) in Au+Au collisions at $\sqrt{s_{NN}} = 200$ GeV for the centrality intervals of 40–60% and 60–80% compared to the lowest-order EPA-QED predictions. Statistical uncertainties are shown as vertical bars, while systematic uncertainties are shown as boxes.

centralities. For real photon interactions, EPA-QED [15, 16] predicts different pair mass distributions for dimuon and dielectron production due to the mass difference, which are shown as solid and dotted lines, respectively. Our data are well described by EPA-QED predictions based on real photon interactions to dimuon.

### *3.3. Low-$p_{\mathrm{T}}$ $J/\psi$ production in Zr+Zr and Ru+Ru collisions*

Figure 4 shows low-$p_{\mathrm{T}}$ $J/\psi$ excess yields scaled with $Z^2$ ($Z$ stands for nucleus charge number) as a function of $Z$. A flat distribution is seen, which reveals that the $J/\psi$ excess yield is proportional to $Z^2$ and not sensitive to the details of the nuclear form factor or the impact parameter. Our data can be described by EPA predictions [17].

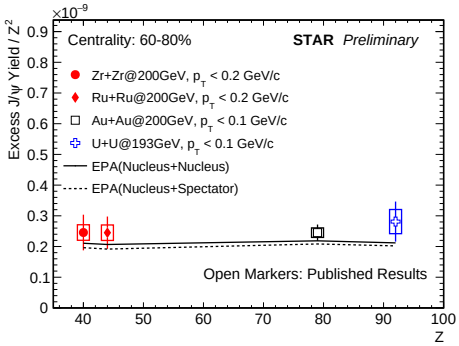


Fig. 4. Low-$p_{\mathrm{T}}$ $J/\psi$ excess yields scaled with $Z^2$ as a function of $Z$ compared to model predictions in Zr+Zr, Ru+Ru, Au+Au, and U+U collisions for the centrality interval of 60–80%. Statistical uncertainties are shown as vertical bars, while systematic uncertainties are shown as boxes. Open markers are extracted from Ref. [9].

## 4. Summary

We report on the measurements of low-$p_{\mathrm{T}}$ $e^+e^-$ and $\mu^+\mu^-$ pairs production in noncentral Au+Au collisions at $\sqrt{s_{NN}} = 54.4$ GeV and $\sqrt{s_{NN}} = 200$ GeV. The observed excesses can be well described by EPA-QED predictions for both channels. There is a $3.7\sigma$ difference in $\sqrt{\langle p_{\mathrm{T}}^2 \rangle}$ of $e^+e^-$ pairs between the measurement at $\sqrt{s_{NN}} = 54.4$ GeV and EPA-QED predictions at $\sqrt{s_{NN}} = 200$ GeV, indicating collision energy dependence and possible final-state effects. The low-$p_{\mathrm{T}}$ $J/\psi$ production in isobaric collisions ($^{96}_{44}$Ru+$^{96}_{44}$Ru, $^{96}_{40}$Zr+$^{96}_{40}$Zr) at $\sqrt{s_{NN}} = 200$ GeV is also measured. $J/\psi$ excess yields scaled with $Z^2$ is flat against $Z$, which reveals that photoproduced $J/\psi$ yields are proportional to $Z^2$ but not sensitive to the details of the nuclear form factor or the impact parameter.

This work was presented for the STAR Collaboration and partially funded by the National Natural Science Foundation of China under grant No. 12075139.

## REFERENCES

[1] M. Gyulassy, L. McLerran, *Nucl. Phys. A* **750**, 30 (2005).
[2] STAR Collaboration (J. Adams *et al.*), *Nucl. Phys. A* **757**, 102 (2005).
[3] F. Krauss, M. Greiner, G. Soff, *Prog. Part. Nucl. Phys.* **39**, 503 (1997).
[4] L. Frankfurt, W. Koepf, M. Strikman, *Phys. Rev. D* **57**, 512 (1998).
[5] STAR Collaboration (J. Adams *et al.*), *Phys. Rev. C* **70**, 031902 (2004).
[6] ALICE Collaboration (B. Abelev *et al.*), *Phys. Lett. B* **718**, 1273 (2013).
[7] STAR Collaboration (J. Adam *et al.*), *Phys. Rev. Lett.* **121**, 132301 (2018).
[8] J. Zhou, *EPJ Web Conf.* **259**, 13014 (2022).
[9] STAR Collaboration (J. Adam *et al.*), *Phys. Rev. Lett.* **123**, 132302 (2019).
[10] X. Wang *et al.*, arXiv:2207.05595 [nucl-th].
[11] J.D. Brandenburg *et al.*, arXiv:2207.02478 [hep-ph].
[12] M. Anderson *et al.*, *Nucl. Instrum. Methods Phys. Res. A* **499**, 659 (2003).
[13] W.J. Llope, *Nucl. Instrum. Methods Phys. Res. A* **661**, S110 (2012).
[14] STAR Collaboration (J. Adam *et al.*), *Phys. Rev. Lett.* **127**, 052302 (2021).
[15] W. Zha, J.D. Brandenburg, Z. Tang, Z. Xu, *Phys. Lett. B* **800**, 135089 (2020).
[16] J.D. Brandenburg, W. Zha, Z. Xu, *Eur. Phys. J. A* **57**, 299 (2021).
[17] W. Zha *et al.*, *Phys. Lett. B* **789**, 238 (2019).